

Possibility of stable octupole deformation in ^{100}Ru

A. Karmakar^{1,2,*}, P. Datta³, Soumik Bhattacharya^{2,4}, Shabir Dar^{2,4,†}, S. Bhattacharyya^{2,4}, G. Mukherjee^{2,4}, H. Pai^{1,2,‡}, S. Basu^{2,4}, S. Nandi^{2,4,§}, S. S. Nayak^{2,4}, Sneha Das^{2,4}, R. Raut⁵, S. S. Ghugre⁵, Sajad Ali⁶, R. Banik⁷, W. Shaikh⁸ and S. Chattopadhyay^{1,2,||}

¹Saha Institute of Nuclear Physics, 1/AF, Bidhan Nagar, Kolkata 700064, India

²Homi Bhabha National Institute, Training School Complex, Anushakti Nagar, Mumbai 400094, India

³Department Of Physics, Ananda Mohan College, Kolkata 700009, India


⁴Variable Energy Cyclotron Centre, Kolkata 700064, India

⁵UGC-DAE Consortium for Scientific Research, Kolkata Centre, Kolkata 700107, India

⁶Department Of Physics, Government General Degree College at Pedong, Kalimpong 734311, India

⁷Institute of Engineering & Management, Sector 5, Kolkata 700091, India

⁸Department of Physics, Mugberia Gangadhar Mahavidyalaya, Purba Medinipur 721425, India

 (Received 12 May 2023; revised 24 March 2024; accepted 16 April 2024; published 8 May 2024)

The high spin level structures of ^{100}Ru have been studied through discrete-line γ -ray spectroscopy. This study reveals the existence of seven interleaved $E1$ transitions between two alternate parity bands of ^{100}Ru , which is a novel observation for this mass region. The measured values of the $B(E1)/B(E2)$ rates exhibit an enhancement and the energy splitting between the alternate parity bands vanishes beyond $I = 16\hbar$. Similar observations for $N = 88$ isotones have been proposed to be an indicator of a phase transition from octupole vibration to octupole deformation. Thus, the present data seem to indicate the presence of octupole deformation in ^{100}Ru beyond $I = 16\hbar$.

DOI: [10.1103/PhysRevC.109.054312](https://doi.org/10.1103/PhysRevC.109.054312)

I. INTRODUCTION

The nuclear rotation was first described by Bohr and Mottelson [1] by considering the nucleus as a quantum droplet which can assume nonspherical shapes. It is well established that the nuclei with proton and/or neutron numbers away from the shell closures exhibit quadrupole deformation and are characterized by the deformation parameter β_2 . These nuclei are either axially symmetric prolate and oblate or can have an asymmetric triaxial shape. However, all these shapes are symmetric with respect to reflection. A reflection asymmetric pear shape of a nucleus can be realized by superimposing octupole deformation (characterized by β_3) on a prolate shape (characterized by β_2) and its rotation for an even-even nucleus is characterized by a unique band structure, where the levels of two alternating parity bands are connected by relatively fast electric dipole ($E1$) transitions. The presence of these transitions is the signature of an intrinsic dipole moment, which arises due to the separation between the center of mass and the center of charge as the concentration of protons is higher

in the region of higher curvature, which is the narrower end of the pear [1].

Such a band structure was first reported in ^{218}Ra [2] and, since then, stable octupole deformation has been reported in a number of even-even isotopes of Ra–Th ($Z \approx 88$ and $N \approx 134$) [3–6] and Sm–Ba ($Z \approx 56$ and $N \approx 88$) nuclei [7–10]. These nuclei possess octupole deformation due to the long-range octupole-octupole correlations among the nucleon orbitals close to the Fermi surface, whose total (J) and orbital (L) angular momenta differ by $3\hbar$. The origin of the band structure of a rotating pear-shaped nucleus can be understood from the variation of the nuclear potential energy of this reflection-asymmetric shape as a function of the octupole deformation parameter [11–14]. The potential energy has two degenerate minima at $\pm\beta_3^{\text{min}}$ separated by a finite barrier at $\beta_3 = 0$. The opposite parity bands correspond to the rotations of the two mirror shapes in these two minima. Thus, for stable octupole deformation, the moments of inertia (MOI) for the two opposite parity bands are expected to be identical. However, as the barrier height is finite, tunneling is possible between the two minima, which leads to parity splitting in the laboratory frame.

There exist other nucleon numbers, namely 34 and 56, where the octupole shape can be favored [11–14]. However, a recent theoretical study concluded that the nuclei in the $A \approx 90$ region are unlikely to possess stable octupole deformation [15]. This has been found to be true as no well-defined rotational band structures have been found in the two $N = 56$ isotones, namely ^{96}Zr ($Z = 40$) [16] and ^{98}Mo ($Z = 42$) [17], although they exhibit the existence of the octupole degree

*anindita.karmakar@saha.ac.in

[†]Present address: Indian Institute of Technology Roorkee, Roorkee, 247667, India.

[‡]Present address: Extreme Light Infrastructure - Nuclear Physics, Horia Hulubei National Institute for R&D in Physics and Nuclear Engineering, Bucharest-Magurele 077125, Romania.

[§]Present address: Physics Division, Argonne National Laboratory, Lemont, Illinois 60439, USA.

^{||}sukalyan.chattopadhyay@saha.ac.in

of freedom. In ^{100}Pd ($Z = 46$), however, a parity doublet structure is observed but the bands become interspaced for $I \geq 16\hbar$, where the Total Routhian Surface (TRS) calculations predict the emergence of the octupole deformation [18]. However, the interleaved $E1$ transitions were not observed in this spin domain. On the other hand, ^{100}Ru ($Z = 44$) has two interspaced opposite parity bands beyond $I = 11\hbar$ [19,20]. This led us to search for the $E1$ transitions between these alternating parity bands, whose presence would indicate a novel excited octupole band in ^{100}Ru .

II. EXPERIMENTAL DETAILS AND RESULTS

The previous experiment on ^{100}Ru [19] was focused to study band termination and thus, the high spin states were populated using the heavy ion ^{36}S beam on a ^{70}Ge target. The γ rays were detected in the EUROGRAM-2 spectrometer [21]. However, only about 3% of the 6×10^8 fourfold coincidence events corresponded to ^{100}Ru , as a large number of residual nuclei were produced in this fusion-evaporation reaction. In the present experiment, excited levels of ^{100}Ru were populated through the fusion-evaporation reaction involving a 98% pure 2 mg/cm² thick ^{100}Mo target and a 50 MeV α beam from the K-130 cyclotron at the Variable Energy Cyclotron Centre (VECC), India. The reaction and the beam energy were chosen such that the yield of ^{100}Ru was nearly 90% of the total fusion cross section. The γ rays were detected by an array of 11 high-purity germanium (HPGe) clover detectors, six of which were placed at 90° to the beam direction, as the dipole emission probability is maximum at this angle. The other two and three detectors were placed in 40° and 125° rings, respectively. About 5×10^9 twofold $\gamma - \gamma$ coincidence data were recorded by the PIXIE-16 digitizer-based data acquisition system [22] and these time-stamped data were sorted into $\gamma - \gamma$ matrices with a coincidence window of 200 ns using the IUCPIX package [22]. The light α beam populated intermediate spin levels ($I \approx 16\hbar$), where we planned to search for the elusive $E1$ transitions by collecting a large data sample.

The symmetric matrix was analyzed using the Radware program ESCL8R [23] to build the partial level scheme of ^{100}Ru , which is shown in Fig. 1. The two new $E3$ transitions observed in the present data are shown in the inset (marked in red) of Fig. 2. It is observed from this figure that the 1036 keV transition is more intense than the 1004 keV transition. Thus, their placements were interchanged with respect to Ref. [19]. In Fig. 2, these two transitions have been labeled in green. The intensities of the γ rays in different gated spectra have been obtained by fitting the observed photopeaks to the Gaussian function using the INGASORT software [24]. The intensities of the interleaved transitions between Band2 and Band3 were estimated from the γ -gated spectra at 90° using the following prescription:

245 keV ($13^- \rightarrow 12^+$): from the two top γ gates of 1036 and 1004 keV.

551 keV ($14^+ \rightarrow 13^-$): from the two top γ gates of 1001 and 1111 keV. This peak is well resolved from the 552 keV transition.

485 keV ($15^- \rightarrow 14^+$): from the immediate top and bottom γ gates of 1004 and 795 keV, respectively.

515 keV ($16^+ \rightarrow 15^-$): from the immediate top γ gate of 1111 keV. In this gate, the contamination due to 516 keV transition ($9^-_{\text{Band4}} \rightarrow 8^+$) was found to be negligible. To validate this observation, the branching ratio for the 14^+ level was also evaluated in the 444 keV gate, which is not in coincidence with the 516 keV transition.

488 keV ($17^- \rightarrow 16^+$): from the two immediate bottom γ gates of 1001 and 795 keV.

623 keV ($18^+ \rightarrow 17^-$): from the two bottom γ gates of 552 and 727 keV since the higher gamma gates of Band3 are contaminated by the 624 keV transition ($9^-_{\text{Band4}} \rightarrow 7^-$). These two gating transitions are not in coincidence with the 624 keV transition.

In the estimation of the $E1/E2$ branching ratios, the enhancement of the intensities of $E1$ transitions observed at 90° has to be corrected for. The correction factor was determined by measuring the branching ratios for (444 and 552 keV), (516 and 624 keV), and (876 and 424 keV) γ rays at 90° and at 125° (at this angle the angular distribution effects are negligible). The weighted mean of the ratio of the branching ratios was found to be 1.58 ± 0.06 . Thus, the $E1/E2$ branching ratios determined at 90° have been divided by this number to correct for the angular distribution effects. The energies and intensities of the observed transitions of ^{100}Ru are listed in Table I. In order to measure the γ -ray multipolarities by the ratio of directional correlations from oriented states (R_{DCO}) method [25], an angle-dependent matrix was constructed with the γ -ray energy detected at 90° along one axis and the coincident γ -ray energy at 125° on the other axis. The linear polarization measurements were also performed to extract the electromagnetic character of the deexciting γ rays using the integrated Polarization from the directional correlation of oriented states method (iPDCO) [26]. The analysis was performed for all the $E2$ transitions of the alternate parity bands except for the top-most transition (1337 keV) of Band3, as the data were insufficient. The measured iPDCO and R_{DCO} values have been plotted in Fig. 3. The $E1$ character of the 444 and 876 keV transitions is evident from the figure. This establishes the negative parity assignment for Band3. It may be noted that iPDCO values for the weak $E1$ transitions were not obtained from the present data set. However, DCO measurements for the 245 ($13^- \rightarrow 12^+$), 485 ($15^- \rightarrow 14^+$), and 515 ($16^+ \rightarrow 15^-$) keV transitions were performed. The R_{DCO} values for the 245 and 485 keV transitions were 0.67 ± 0.07 and 0.65 ± 0.09 , when gated on the $\Delta I = 2$ transitions of 834 and 795 keV, respectively. This value was 1.06 ± 0.10 for 515 keV when gated on the $\Delta I = 1$ transition of 444 keV. All these values match with the calculated R_{DCO} value for a pure $\Delta I = 1$ transition for the given detector geometry. Thus, the dipole transitions between the positive parity Band2 and negative parity Band3 have been assigned as $E1$ since the $M2$ mixing is negligible. The measured R_{DCO} and iPDCO values are tabulated in Table I. The present results are in agreement with previous measurements [19,27].

The $B(E1)/B(E2)$ rates were determined from the following relation:

$$\frac{B(E1, I_i \rightarrow I_i - 1) \downarrow}{B(E2, I_i \rightarrow I_i - 2) \downarrow} = \frac{1}{1.3 \times 10^6} \frac{I(E1) E_\gamma^5(E2)}{I(E2) E_\gamma^3(E1)} \text{ fm}^{-2},$$

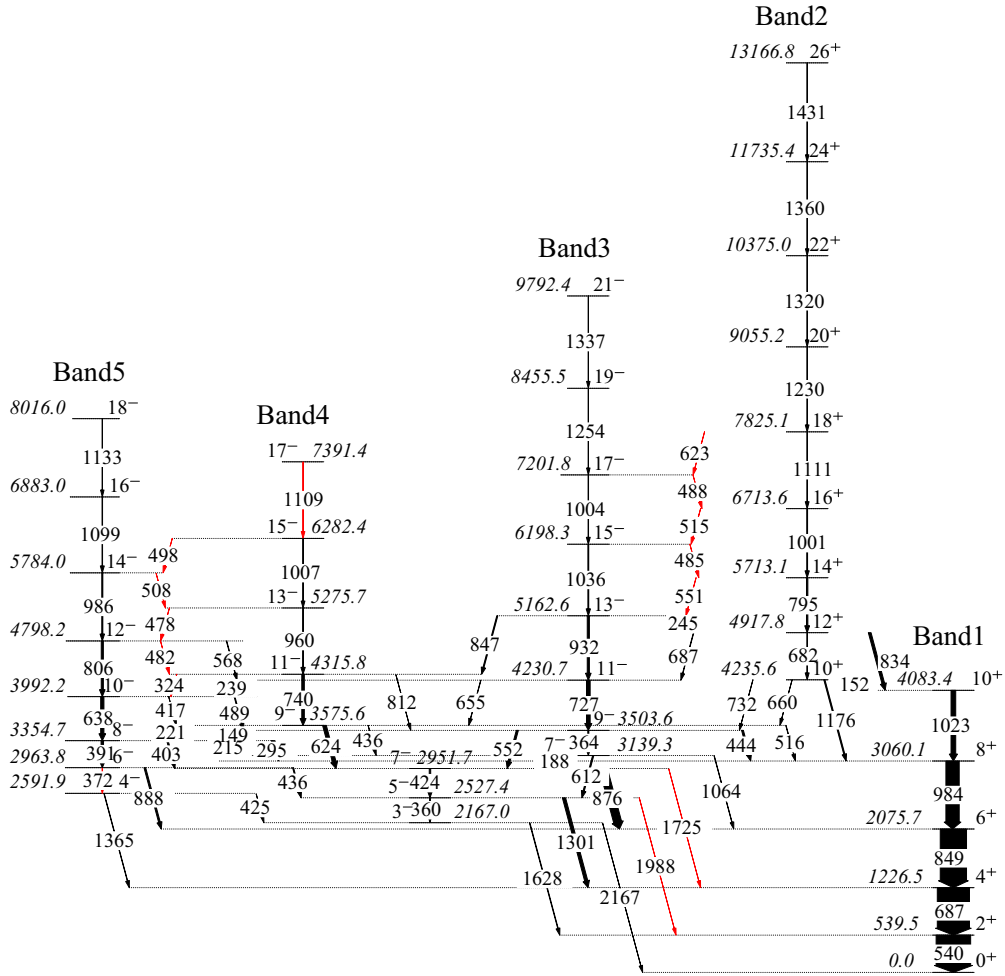


FIG. 1. The partial level scheme of ^{100}Ru established from the present work. Seven interleaved transitions between Band2 and Band3 were observed in the present work. The level and transition energies are expressed in keV. γ -ray energies have been rounded off to their closest integer. The thicknesses of the arrows are proportional to the relative intensities of the deexciting γ rays. The transitions marked in red are newly observed in the present data set. The high spin levels beyond $I = 20\hbar$ were reported in Ref. [19] but not observed in the present experiment.

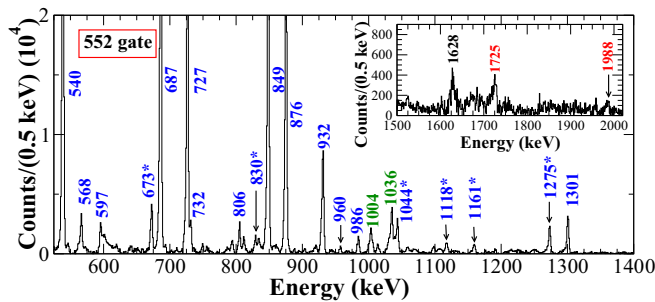


FIG. 2. The γ -ray spectrum in coincidence with the 552 keV ($9^- \rightarrow 7^-$) transition. The γ energies have been rounded off to the nearest integer. The higher energy section of the gated spectrum is shown in the inset. The γ rays marked with * are from other excited levels of ^{100}Ru [27], which are not part of the partial level scheme shown in Fig. 1.

where the energies of the γ rays (E_γ) are expressed in MeV and $I(E1)/I(E2)$ is the measured branching ratio. The $B(E1)/B(E2)$ ratios for low spin levels of ^{100}Ru are listed in Table II. The $E1$ and $E2$ branching ratios for each level of the alternate parity bands were estimated from two different γ -gated spectra. The values listed in Table III are the weighted average of the two values obtained from the two independent γ gates. These gated spectra are shown in Fig. 4.

III. DISCUSSION

In Fig. 1, Band1 is the ground state band of ^{100}Ru , which corresponds to the vacuum configuration for this even-even nucleus. Band2 has been proposed to originate from the rotational alignment (RAL) of a pair of neutrons in the $h_{11/2}$ orbitals [19]. This is observed as a sharp discontinuity in the band structure of the ground state Band1 at $I = 10\hbar$, beyond which Band2 (the s band of Band1) becomes favored in energy. This phenomenon [28] happens when the Coriolis

TABLE I. The energy (E_γ) and the relative intensity (I_γ) of the γ rays of ^{100}Ru along with the spin and parity of the initial (J_π^i) and the final (J_π^f) states, measured values of R_{DCO} , Δ_{iPDCO} , and the energy of the initial state (E_i) are shown. R_{DCO} values are obtained with gates on pure quadrupole transitions except as noted. The quoted uncertainties in the intensities include statistical and fitting errors only. The systematic error due to the efficiency determination has been estimated to be around 3%.

E_i (keV)	E_γ (keV)	$J_\pi^i \rightarrow J_\pi^f$	I_γ	R_{DCO}	Δ_{iPDCO}	Type
539.5(2)	539.5(2)	$2^+ \rightarrow 0^+$	100.0(3)	1.00(1)	0.11(1)	$E2$
1226.4(1)	686.9(1)	$4^+ \rightarrow 2^+$	93.2(4)	0.99(1)	0.09(1)	$E2$
2075.7(1)	849.2(2)	$6^+ \rightarrow 4^+$	76.1(3)	1.02(1)	0.08(1)	$E2$
2167.0(3)	1627.5(4)	$3^- \rightarrow 2^+$	1.42(3)			$E1^a$
	2167.0(3)	$3^- \rightarrow 0^+$	0.46(7)			$E3^a$
2527.4(3)	360.4(5)	$5^- \rightarrow 3^-$	0.73(9)	1.03(5)		$E2^a$
	1300.9(3)	$5^- \rightarrow 4^+$	9.02(2)	0.70(3)	0.05(1)	$E1$
	1987.9(3)	$5^- \rightarrow 2^+$	0.12(3)			$E3^b$
2951.9(2)	424.3(5)	$7^- \rightarrow 5^-$	4.20(44)	0.99(2)	0.07(2)	$E2$
	876.0(2)	$7^- \rightarrow 6^+$	23.19(22)	0.65(1)	0.09(1)	$E1$
	1725.2(4)	$7^- \rightarrow 4^+$	0.24(7)			$E3^b$
2591.9(2)	1365.4(4)	$4^- \rightarrow 4^+$	1.01(1)			$E1^a$
	424.9(4)	$4^- \rightarrow 3^-$	0.48(5)			$M1 + E2^a$
2963.8(1)	371.9(5)	$6^- \rightarrow 4^-$	1.66(17)	1.02(4)		$E2^a$
	888.1(2)	$6^- \rightarrow 6^+$	4.77(3)	0.78(2)	-0.12(8)	$E1$
	436.4(3)	$6^- \rightarrow 5^-$	2.71(2)	0.84(3)		$M1 + E2$
3060.1(2)	984.4(2)	$8^+ \rightarrow 6^+$	38.48(24)	0.99(1)	0.08(1)	$E2$
3139.5(4)	187.6(3)	$7^- \rightarrow 7^-$	1.94(20)			
	1063.6(2)	$7^- \rightarrow 6^+$	0.75(8)	0.62(4)		$E1^a$
	611.9(6)	$7^- \rightarrow 5^-$	3.36(5)	1.03(4)		$E2^a$
3503.6(2)	364.3(3)	$9^- \rightarrow 7^-$	4.13(39)	1.02(3)		$E2^a$
	443.5(3)	$9^- \rightarrow 8^+$	5.13(31)	0.66(1)	0.08(1)	$E1$
	551.9(4)	$9^- \rightarrow 7^-$	5.78(34)	0.97(4)	0.10(3)	$E2$
	148.9(3)	$9^- \rightarrow 8^-$	1.87(2)	0.71(8)		$M1 + E2^a$
3354.7(1)	390.9(3)	$8^- \rightarrow 6^-$	7.13(3)	1.00(2)		$E2^a$
	294.6(5)	$8^- \rightarrow 8^+$	0.54(6)			$E1^a$
	403.0(3)	$8^- \rightarrow 7^-$	4.10(3)			$M1 + E2^a$
	215.4(3)	$8^- \rightarrow 7^-$	0.44(4)	0.71(4)		D^b
3575.6(2)	623.9(4)	$9^- \rightarrow 7^-$	10.51(50)	1.01(3)	0.08(3)	$E2$
	515.5(3)	$9^- \rightarrow 8^+$	0.92(4)	0.69(4)	0.08(4)	$E1$
	436.3(3)	$9^- \rightarrow 7^-$	0.52(6)	1.05(6)		$E2$
	220.9(4)	$9^- \rightarrow 8^-$	0.08(1)			
3992.2(3)	637.5(2)	$10^- \rightarrow 8^-$	9.35(3)	0.98(3)	0.06(4)	$E2$
	416.6(3)	$10^- \rightarrow 9^-$	0.23(7)	0.74(5)	-0.04(5)	$M1 + E2^b$
	488.6(4)	$10^- \rightarrow 9^-$	2.20(8)	0.74(1)	-0.05(2)	$M1 + E2$
4083.4(1)	1023.3(2)	$10^+ \rightarrow 8^+$	13.5(2)	0.99(1)	0.09(1)	$E2$
4230.7(1)	727.1(2)	$11^- \rightarrow 9^-$	6.57(4)	1.00(3)	0.07(2)	$E2$
	655.1(1)	$11^- \rightarrow 9^-$	0.76(2)	1.02(2)	0.06(4)	$E2^b$
	238.5(3)	$11^- \rightarrow 10^-$	1.07(4)	0.73(7)		$M1 + E2^a$
4235.6(4)	1175.8(2)	$10^+ \rightarrow 8^+$	3.11(13)	1.03(2)	0.13(3)	$E2^b$
	152.2(3)	$10^+ \rightarrow 10^+$	0.28(5)			
	732.0(2)	$10^+ \rightarrow 9^-$	0.21(7)			
	660.0(4)	$10^+ \rightarrow 9^-$	0.05(1)			
4315.8(3)	740.2(3)	$11^- \rightarrow 9^-$	7.33(60)	1.08(4)	0.11(4)	$E2$
	323.6(3)	$11^- \rightarrow 10^-$	0.09(2)	0.60(7)	-0.22(16)	$M1 + E2^b$
	812.2(3)	$11^- \rightarrow 9^-$	0.34(3)	1.07(5)		Q^b
4798.2(2)	806.0(3)	$12^- \rightarrow 10^-$	6.07(4)	0.99(4)	0.07(5)	$E2$
	482.4(3)	$12^- \rightarrow 11^-$	0.35(4)	0.72(5)	-0.09(6)	$M1 + E2^b$
	567.5(4)	$12^- \rightarrow 11^-$	1.20(3)	0.77(2)	-0.06(4)	$M1 + E2^b$
4917.8(2)	682.2(2)	$12^+ \rightarrow 10^+$	1.41(2)	1.05(3)	0.09(4)	$E2^b$
	687.1(4)	$12^+ \rightarrow 11^-$	0.34(8)			$E1^{a,b}$
	834.4(5)	$12^+ \rightarrow 10^+$	7.65(10)	0.98(2)	0.05(3)	$E2$

TABLE I. (Continued.)

E_i (keV)	E_γ (keV)	$J_\pi^i \rightarrow J_\pi^f$	I_γ	R_{DCO}	Δ_{iPDCO}	Type
5162.6(3)	931.9(2)	$13^- \rightarrow 11^-$	6.19(4)	1.00(1)	0.08(1)	$E2$
	244.8(4)	$13^- \rightarrow 12^+$	0.017(4)	0.67(7)		$E1^b$
	846.8(4)	$13^- \rightarrow 11^-$	2.86(13)	1.06(1)	0.05(4)	$E2^b$
5275.7(2)	959.9(4)	$13^- \rightarrow 11^-$	2.52(7)	1.00(4)	0.07(4)	$E2$
	477.5(5)	$13^- \rightarrow 12^-$	0.27(3)	0.74(6)	0.04(11)	$M1 + E2^b$
5713.1(1)	795.3(3)	$14^+ \rightarrow 12^+$	3.91(2)	0.99(1)	0.13(2)	$E2$
	550.5(4)	$14^+ \rightarrow 13^-$	0.15(4)			$E1^{a,b}$
5784.0(4)	985.8(3)	$14^- \rightarrow 12^-$	3.03(4)	1.03(6)	0.04(3)	$E2$
	508.3(4)	$14^- \rightarrow 13^-$	0.11(2)	0.55(6)	-0.21(13)	$M1 + E2^b$
6198.3(2)	1035.7(3)	$15^- \rightarrow 13^-$	2.39(2)	1.01(3)	0.02(1)	$E2$
	485.2(4)	$15^- \rightarrow 14^+$	0.037(8)	0.65(9)		$E1^b$
6282.4(6)	1006.7(5)	$15^- \rightarrow 13^-$	0.85(6)	0.97(7)	0.05(3)	$E2^b$
	498.4(4)	$15^- \rightarrow 14^-$	0.09(2)	0.58(6)	-0.37(23)	$M1 + E2^b$
6713.6(1)	1000.5(3)	$16^+ \rightarrow 14^+$	2.31(2)	1.00(1)	0.21(2)	$E2$
	515.3(3)	$16^+ \rightarrow 15^-$	0.04(1)	1.06(10) ^c		$E1^b$
6883.0(5)	1099.2(4)	$16^- \rightarrow 14^-$	1.44(20)	0.96(4)	0.15(3)	$E2$
7201.8(2)	1003.5(4)	$17^- \rightarrow 15^-$	1.24(2)	0.99(3)	0.05(4)	$E2$
	488.2(5)	$17^- \rightarrow 16^+$	0.03(1)			$E1^{a,b}$
7391.4(6)	1109.1(5)	$17^- \rightarrow 15^-$	0.51(20)	1.01(5)	0.12(8)	$E2^b$
7825.1(2)	1111.4(4)	$18^+ \rightarrow 16^+$	1.13(1)	1.03(3)	0.04(3)	$E2$
	623.3(4)	$18^+ \rightarrow 17^-$	0.06(2)			$E1^{a,b}$
8016.0(5)	1133.0(4)	$18^- \rightarrow 16^-$	0.32(3)	0.96(6)	0.06(4)	$E2$
8455.5(5)	1253.7(5)	$19^- \rightarrow 17^-$	0.28(2)	1.02(4)	0.11(8)	$E2^b$
9055.2(3)	1229.5(5)	$20^+ \rightarrow 18^+$	0.81(3)	1.01(3)	0.09(3)	$E2$

^aThe $M2$ mixing has been assumed to be negligible following the discussions given in the text.

^bNew measurement from current data.

^cGate on dipole transition ($444 \text{ keV } 9^- \rightarrow 8^+$).

interaction decouples a pair of nucleons and aligns their angular momentum vectors along the rotational axis.

The lowest observed negative parity level in ^{100}Ru is 3^- . The hindrance factor for $E1$ transition estimated from the lifetime measurement for this level is 1.0×10^{-5} [20]. A similar retardation factor of 1.2×10^{-5} has been estimated for the 5^-

level using the observed intensity ratio of the $E1$ and $E2$ transitions from this level and assuming $Q_0 \approx 200 e \text{ fm}^2$ for ^{100}Ru following the systematics of the $B(E2, 2^+ \rightarrow 0^+)$ transition rate [29]. This hindrance is similar to the $(1-2) \times 10^{-5}$ factor observed for the single neutron transitions in odd Cd isotopes [18], which indicates that there is no permanent octupole

TABLE II. $E1$ and $E2$ branching ratios and the estimated values of $B(E1)/B(E2)$ for the low spin levels of ^{100}Ru . The γ energies were taken in MeV for calculating the $B(E1)/B(E2)$ ratios.

$E_{\text{level}} [J^\pi]$ (keV)	E_γ (keV)	γ gates	$I(E1)/I(E2)$	$B(E1)/B(E2)$ (10^{-8} fm^{-2})
2527 [5^-]	1301 ($E1$)	552	12.34 ± 1.51	2.61 ± 0.32
	360 ($E2$)			
2964 [6^-]	888 ($E1$)	391	2.87 ± 0.30	2.25 ± 0.24
	372 ($E2$)			
2952 [7^-]	876 ($E1$)	552	5.52 ± 0.57	8.63 ± 0.90
	424 ($E2$)			
3355 [8^-]	295 ($E1$)	638	0.08 ± 0.01	2.08 ± 0.25
	391 ($E2$)			
3504 [9^-]	444 ($E1$)	727	1.24 ± 0.14	6.94 ± 0.76
	364 ($E2$)			
3576 [9^-]	516 ($E1$)	740	0.09 ± 0.01	4.63 ± 0.29
	624 ($E2$)			

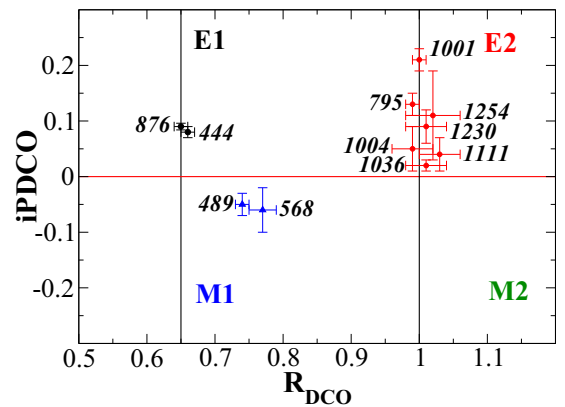


FIG. 3. The measured values of ratio of directional correlations from oriented states (R_{DCO}) and integrated polarization from the directional correlation of oriented states (iPDCO) for different γ transitions of ^{100}Ru . The vertical lines represent the calculated R_{DCO} values of 0.65 and 1.0 for pure $\Delta I = 1$ and $\Delta I = 2$ transitions, respectively, in a stretched $E2$ gate.

TABLE III. $E1$ and $E2$ branching ratios and the estimated values of $B(E1)/B(E2)$ for the levels of the alternate parity band. The γ energies were taken in MeV for calculating the $B(E1)/B(E2)$ ratios. The evaluated branching ratio is the weighted average of the values obtained from the two independent gates.

$E_{\text{level}} [J^\pi]$ (keV)	E_γ (keV)	γ gates	$I(E1)/I(E2)$ (10^{-2})	$B(E1)/B(E2)$ (10^{-8} fm^{-2})
4918 [12 ⁺]	687 ($E1$) 682 ($E2$)	795 and 687	24.21 ± 5.37	8.47 ± 1.88
5163 [13 ⁻]	245 ($E1$) 932 ($E2$)	1036 and 1004	0.27 ± 0.05	9.84 ± 1.93
5713 [14 ⁺]	551 ($E1$) 795 ($E2$)	1111 and 1001	3.93 ± 1.04	5.88 ± 1.55
6198 [15 ⁻]	485 ($E1$) 1036 ($E2$)	1004 and 795	1.54 ± 0.35	12.56 ± 2.83
6714 [16 ⁺]	515 ($E1$) 1001 ($E2$)	1111 and 444	1.72 ± 0.41	9.75 ± 2.35
7202 [17 ⁻]	488 ($E1$) 1004 ($E2$)	1001 and 795	2.53 ± 0.80	17.07 ± 5.41
7825 [18 ⁺]	623 ($E1$) 1111 ($E2$)	727 and 552	5.17 ± 1.56	27.92 ± 8.40

deformation in ^{100}Ru at low spins. Thus, the presence of the $E3$ transitions from the low spin negative parity levels indicates that these levels originate due to the collective octupole vibration around a reflection symmetric shape.

At higher spins, three negative parity bands are seen in Fig. 1. Interleaved $M1$ transitions have been observed till $I^\pi = 15^-$ between Band4 and Band5 while these transitions with Band3 are observed only up to $I^\pi = 11^-$ although Band3 is the

negative parity yrast sequence. This observation indicates that Band4 and Band5 are signature partners while the presence of $M1$ transitions between Band3 and Band5 is probably due to the mixing of 9^- and 11^- levels of Band3 and Band4 as they lie very close in energy (≈ 100 keV). This assumption is supported by the large $B(E2)_{\text{out}}/B(E2)_{\text{in}}$ value [0.74(4)] observed for the 13^- level of Band3 evaluated from the observed intensities of the 847 (between 5162.6 and 4315.8 keV levels) and 932 keV (between 5162.6 and 4230.7 keV levels) transitions. In the two previous experiments and from the present data set, no unfavored signature partner of Band3 could be identified. However, its absence may also indicate that this band is shifted to higher energies due to the large signature splitting.

In order to explore the presence of the octupole correlations in ^{100}Ru , the ratio of the interband $E1$ and intraband $E2$ transition rates, $B(E1)_{\text{out}}/B(E2)_{\text{in}}$, have been plotted in Fig. 5.

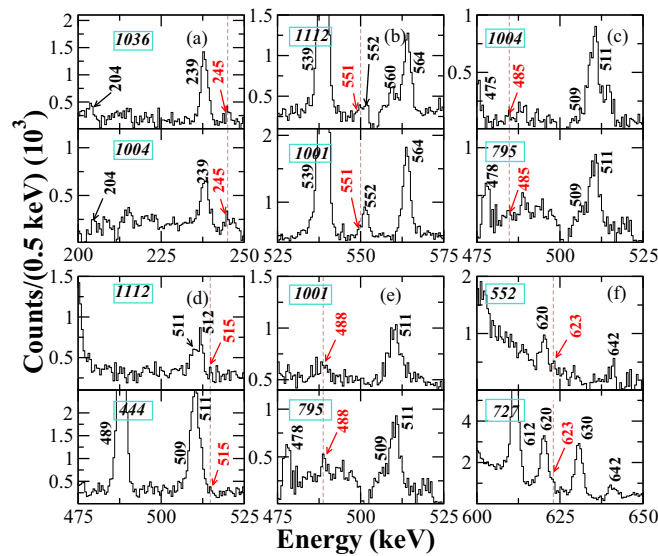


FIG. 4. Coincident γ spectra observed with the detectors of the 90° ring. The $E1$ transitions connecting Band2 and Band3 are marked by the dotted line. Each $E1$ transition is shown in two γ -gated spectra. The numbers in the rectangular box represent the γ -ray energy of the gating transitions. The γ energies have been rounded off to their closest integer.

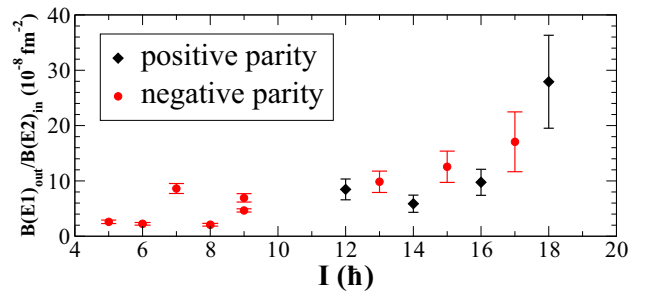


FIG. 5. Ratios of the interband $E1$ and the intraband $E2$ transition rates from the excited levels of ^{100}Ru as a function of spin, I . The lower value of the ratio for the 9^- level corresponds to Band4. The values for $I \leq 9\hbar$ corresponds to $\Delta\nu = 2$ $E1$ transitions between Band3 and Band1, while, for the higher spins, $\Delta\nu = 0$ $E1$ transitions between Band3 and Band4 are considered.

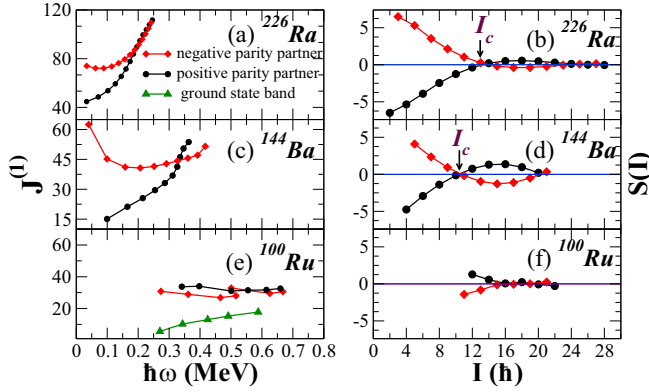


FIG. 6. Moment of inertia $J^{(1)}$ and parity splitting index $S(I)$ for the positive (black dots) and the negative parity (red diamonds) partner bands of ^{226}Ra , ^{144}Ba , and ^{100}Ru are plotted on the left and right panels as a function of rotational frequency (ω) and angular momentum I , respectively.

These values for the 6^- ($E_x = 2963.8$ keV) and 8^- ($E_x = 3354.7$ keV) levels have been extracted by assuming a pure $E1$ character for the $6^- \rightarrow 6^+$ and $8^- \rightarrow 8^+$ transitions and were found to be similar to that for the 5^- level ($E_x = 2527.4$ keV). For the 7^- ($E_x = 2951.9$ keV), 9_{Band3}^- ($E_x = 3503.6$ keV), and 9_{Band4}^- ($E_x = 3575.6$ keV) levels, the observed retardation factor lies in the range $(4-7) \times 10^{-5}$ assuming $Q_0 = 200 e \text{ fm}^2$. This apparent increase can be understood from the calculations of $E1$ rates by Hamamoto and Sagawa [30] between the two-quasineutron band ($\nu = 2$) and ground state band ($\nu = 0$), which predict $B(E1)$ values as large as $10^{-4} e^2 \text{ fm}^2$ for $\Delta\nu = 2$ $E1$ transitions without incorporating octupole deformation. The calculations were also performed for $\Delta\nu = 0$ transitions and the rates were found to be considerably smaller than the $\Delta\nu = 2$ transitions. However, these calculated values underestimated the observed $B(E1)$ values by one to three orders of magnitude in the odd- A rare-earth nuclei, which are stable against octupole deformation. It has been proposed [31] that such large enhancement in the $E1$ rates may arise due to the particle octupole vibrational coupling and the observed rates can be reproduced by tuning the amplitude of an additional term in the $E1$ transition operator, which accounts for the octupole vibrations in quadrupole-deformed nuclei. However, in all these cases, the two opposite parity bands are not interspaced and their moments of inertia are different. In the mass 100 region, interspaced opposite parity bands have been reported in ^{104}Pd [32], ^{103}Pd [33], and ^{102}Ru [34] following the neutron $h_{11/2}$ alignment. But in these cases also the moments of inertia (MOI) of the two bands are significantly different. This difference indicates that the negative and the positive parity bands in these nuclei originate from $\nu\{[d_{5/2}/g_{7/2}] \otimes h_{11/2}\}$ and $\nu h_{11/2}^2$ configurations, respectively. In addition, the interleaved transitions have not been reported between the alternate parity bands. Thus, ^{100}Ru is the first nucleus in the $A \approx 100$ region for which seven interleaved $E1$ transitions have been observed and the moments of inertia of the two alternate parity bands are found to be nearly identical for $I > 16\hbar$ [as seen from Fig. 6(e)]. These observations can

be simultaneously accounted for by considering the alignment to occur in the mixed parity orbitals of $\{[d_{5/2}/g_{7/2}]/h_{11/2}\}$ in the intrinsic frame and the parity partners originate due to the parity projection in the laboratory frame. Such a configuration in ^{100}Ru is possible due to the proximity of the octupole driving orbitals of $h_{11/2}-d_{5/2}$ states for $N = 56$ [35]. It may be noted that the emergence of stable octupole deformation above the first band crossing has already been reported in even-even Lanthanide nuclei [36–38]. The level energies and $B(E1)$ transition probabilities for $N = 88$ isotones have been calculated by Garrote *et al.* [39] within the framework of the cranked Hartree-Fock-Bogoliubov approximation with the parity breaking Gogny interaction. The comparison with the observed energy splitting between the alternate parity levels and the $B(E1)/B(E2)$ rates shows a good agreement. These calculations indicate a phase transition from an octupole vibration to an octupole deformation at a higher spin ($I \approx 10\hbar$) in $N = 88$ isotones, which is characterized by the vanishing of the parity splitting and the enhancement of the $B(E1)/B(E2)$ rates. It is interesting to note that the $B(E1)/B(E2)$ rates for the alternate parity bands at low spins ($I \leq 16\hbar$) of ^{100}Ru are similar to those observed from the octupole vibrational level of 7^- ($E_x = 2951.9$ keV) (as seen from Fig. 5). But on the other hand, the rates increase significantly and also the signature splitting vanishes beyond $I = 16\hbar$ [as seen from Fig. 6(f)]. Thus, from the perspective of Ref. [39], ^{100}Ru seems to exhibit the octupole vibration to octupole deformation phase transition at $I = 16\hbar$.

However, it is important to note that the weighted average value of $B(E1)/B(E2)$ beyond $I = 16\hbar$ is $2.0(5) \times 10^{-7} \text{ fm}^{-2}$, which is an order of magnitude smaller than those observed in the lanthanide and actinide regions [38,40]. This indicates that the electric dipole transitions are less enhanced in ^{100}Ru and thus, the octupole deformation is lower. On the other hand, the $\nu h_{11/2}^2$ and $\nu\{[d_{5/2}/g_{7/2}]/h_{11/2}\}$ assignments for Band2 and Band3 respectively, cannot be ruled out. Thus, to establish the stable octupole deformation in ^{100}Ru , it is essential to measure the level lifetimes for the alternate parity bands and compare the measured $B(E1)$ values with the calculated rates for the two separate configurations for Band2 and Band3.

In order to explore the rotational characteristics of the two alternate parity bands of ^{100}Ru , the moments of inertia of the parity partner bands of two well-known pear-shaped nuclei, namely ^{226}Ra [5] and ^{144}Ba [10], have been compared with those of ^{100}Ru on the left panel of Fig. 6. On the right panel, the values of parity splitting indices, $S(I^+)$ and $S(I^-)$ have been plotted, where $S(I)$ is defined as the difference of the energy difference of the I , $(I-1)$, and $(I-2)$ levels [41]. For ^{226}Ra , the value of both the parity indices becomes zero at $I_c = 12\hbar$, which indicates the onset of strong octupole correlations [41]. At the corresponding frequency ($\hbar\omega = 0.18$ MeV), the MOI values of both the bands become similar as shown in Fig. 6(a). This marks the onset of stable octupole deformation in ^{226}Ra [14], and beyond I_c the negative parity levels become favored in energy. This phenomenon of parity inversion in the nuclei of the actinide region has been explored by Jolos *et al.* [42] within the framework of the particle-rotor coupling model. These calculations indicate that the intrinsic configuration for the alternating parity bands changes from a

fully paired configuration ($K = 0$, where K is the projection of I along the symmetry axis of the nucleus) before the parity inversion to one with rotationally aligned nucleons ($K \neq 0$) after the inversion. Thus, the rotational alignment leads to the stabilization of octupole deformation as the pairing correlations become weaker [40]. With increasing spin, the potential barrier height at $\beta_3 = 0$ increases and the parity splitting due to the tunneling between the two minima vanishes beyond the $I = 23\hbar$ in ^{226}Ra , as seen in Fig. 6(b).

The nature of the $S(I)$ plot for ^{144}Ba is very similar to that of ^{226}Ra as seen from [Fig. 6(d)]. The parity inversion happens around $I = 10\hbar$ [38], where the first band crossing takes place and, beyond $I = 20\hbar$, the parity splitting vanishes. However, the MOI of the alternate parity bands continue to be significantly different till the highest observed frequencies as seen from Fig 6(c) and in this respect, the behavior is different from ^{226}Ra .

The MOI and $S(I)$ plots for ^{100}Ru are distinct from the above two cases as seen in Fig. 6. It is observed from Fig. 6(e) that the MOI values of the two parity bands are similar over the entire range of observed spins. This is the consequence of the RAL configuration for the alternate parity bands of ^{100}Ru , as the pairing correlation becomes substantially weaker. It may be noted that the MOI values of the pear-shaped odd-mass nuclei, for example ^{223}Th [43] and ^{225}Th [44], also exhibit a similar weak dependence on rotational frequency due to the presence of the odd nucleon, which lowers the pairing correlations due to Pauli blocking.

At lower spins, $12\hbar \leq I \leq 16\hbar$, the difference in the MOI values is probably due to the octupole vibration. This assumption is consistent with the observed $B(E1)/B(E2)$ values in this spin range. Beyond $I = 16\hbar$, the MOI values for the alternate parity bands become nearly identical and the parity splitting vanishes as seen from Figs. 6(e) and 6(f), respectively. This observation, along with the observed

increase in the $B(E1)/B(E2)$ values (as seen from Fig. 5), seems to indicate the onset of stable octupole deformation in ^{100}Ru beyond $I = 16\hbar$.

IV. SUMMARY

In summary, seven interleaved $E1$ transitions have been observed between the two alternate parity bands of ^{100}Ru , whose moments of inertia are nearly identical. The enhancement of the $B(E1)_{\text{out}}/B(E2)_{\text{in}}$ rates and the vanishing of the parity splitting beyond $I = 16\hbar$ seem to indicate the emergence of stable octupole deformation in ^{100}Ru based on a RAL configuration. However, the order of magnitude smaller value of $B(E1)_{\text{out}}/B(E2)_{\text{in}}$ than those observed in the lanthanide and actinide regions does not rule out the assignment of $\nu[\{d_{5/2}/g_{7/2}\} \otimes h_{11/2}]$ configuration of Band3 and $\nu h_{11/2}^2$ configuration of Band2. Thus, the direct measurement of the $B(E1)$ rates in ^{100}Ru , and the calculations of these rates assuming the two distinct configurations for Band2 and Band3, are necessary to establish stable octupole deformation in ^{100}Ru .

ACKNOWLEDGMENTS

The authors would like to thank the operational staff of the K-130 cyclotron at VECC for providing a good quality beam as well as necessary support during the pandemic period. We are thankful to A. Navin for stimulating discussions. The authors are thankful to the Department of Atomic Energy and the Department of Science and Technology, Government of India for providing the necessary funding for the clover array. A.K. acknowledges the grant from the Council of Scientific & Industrial Research (CSIR) [File No. 09/489(0121)/2019-EMR-I], Government of India.

-
- [1] A. Bohr and B. R. Mottelson, *Nuclear Structure* (World Scientific Publishing Company, 1998).
- [2] J. Fernández-Niello, H. Puchta, F. Riess, and W. Trautmann, *Nucl. Phys. A* **391**, 221 (1982).
- [3] L. P. Gaffney, P. A. Butler, M. Scheck, A. B. Hayes, F. Wenander, M. Albers, B. Bastin, C. Bauer, A. Blazhev, S. Bönig, N. Bree, J. Cederkäll, T. Chupp, D. Cline, T. E. Cocolios, T. Davinson, H. De Witte, J. Diriken, T. Grahn, A. Herzan *et al.*, *Nature (London)* **497**, 199 (2013).
- [4] M. M. R. Chishti, D. O'Donnell, G. Battaglia, M. Bowry, D. A. Jaroszynski, B. S. Nara Singh, M. Scheck, P. Spagnoletti, and J. F. Smith, *Nat. Phys.* **16**, 853 (2020).
- [5] J. F. C. Cocks, P. A. Butler, K. J. Cann, P. T. Greenlees, G. D. Jones, S. Asztalos, P. Bhattacharyya, R. Broda, R. M. Clark, M. A. Deleplanque, R. M. Diamond, P. Fallon, B. Fornal, P. M. Jones, R. Julin, T. Lauritsen, I. Y. Lee, A. O. Macchiavelli *et al.*, *Phys. Rev. Lett.* **78**, 2920 (1997).
- [6] P. A. Butler, L. P. Gaffney, P. Spagnoletti, K. Abrahams, M. Bowry, J. Cederkäll, G. de Angelis, H. De Witte, P. E. Garrett, A. Goldkuhle, C. Henrich, A. Illana, K. Johnston, D. T. Joss, J. M. Keatings, N. A. Kelly, M. Komorowska, J. Konki, T. Kröll *et al.*, *Phys. Rev. Lett.* **124**, 042503 (2020).
- [7] B. Bucher, S. Zhu, C. Y. Wu, R. V. F. Janssens, R. N. Bernard, L. M. Robledo, T. R. Rodríguez, D. Cline, A. B. Hayes, A. D. Ayangeakaa, M. Q. Buckner, C. M. Campbell, M. P. Carpenter, J. A. Clark, H. L. Crawford, H. M. David, C. Dickerson, J. Harker, C. R. Hoffman, B. P. Kay *et al.*, *Phys. Rev. Lett.* **118**, 152504 (2017).
- [8] R. K. Sheline and P. C. Sood, *Phys. Rev. C* **34**, 2362(R) (1986).
- [9] W. Andrejtscheff, C. Doll, F. Bečvář, and H. G. Börner, *Phys. Lett. B* **437**, 249 (1998).
- [10] S. J. Zhu, E. H. Wang, J. H. Hamilton, A. V. Ramayya, Y. X. Liu, N. T. Brewer, Y. X. Luo, J. O. Rasmussen, Z. G. Xiao, Y. Huang, G. M. Ter-Akopian, and T. Oganessian, *Phys. Rev. Lett.* **124**, 032501 (2020).
- [11] P. A. Butler and W. Nazarewicz, *Rev. Mod. Phys.* **68**, 349 (1996).
- [12] P. A. Butler, *J. Phys. G* **43**, 073002 (2016).
- [13] P. A. Butler, *Proc. R. Soc. A* **476**, 20200202 (2020).

- [14] I. Ahmad and P. A. Butler, *Annu. Rev. Nucl. Part. Sci.* **43**, 71 (1993).
- [15] Y. Cao, S. E. Agbemava, A. V. Afanasjev, W. Nazarewicz, and E. Olsen, *Phys. Rev. C* **102**, 024311 (2020).
- [16] Ł. W. Iskra, R. Broda, R. V. F. Janssens, M. P. Carpenter, B. Fornal, T. Lauritsen, T. Otsuka, T. Togashi, Y. Tsunoda, W. B. Walters, and S. Zhu, *Phys. Lett. B* **788**, 396 (2019).
- [17] S. Lalkovski, S. Ilieva, A. Minkova, N. Minkov, T. Kutsarova, A. Lopez-Martens, A. Korichi, H. Hübel, A. Görgen, A. Jansen, G. Schönwasser, B. Herskind, M. Bergström, and Z. Podolyák, *Phys. Rev. C* **75**, 014314 (2007).
- [18] G. E. Perez, D. Sohler, A. Algora, Zs. Dombrádi, B. M. Nyakó, J. Timár, L. Zolnai, R. Wyss, J. Cederkäll, A. Johnson, A. Kerek, W. Klamra, L.-O. Norlin, M. Lipoglavšek, C. Fahlander, A. Likar, M. Palacz, A. Atac, J. Nyberg, J. Persson *et al.*, *Nucl. Phys. A* **686**, 41 (2001).
- [19] J. Timár, J. Gizon, A. Gizon, D. Sohler, B. M. Nyakó, L. Zolnai, A. J. Boston, D. T. Joss, E. S. Paul, A. T. Semple, C. M. Parry, and I. Ragnarsson, *Phys. Rev. C* **62**, 044317 (2000).
- [20] B. Singh and J. Chen, *Nucl. Data Sheets* **172**, 1 (2021).
- [21] P. J. Nolan, F. A. Beck, and D. B. Fossan, *Annu. Rev. Nucl. Part. Sci.* **44**, 561 (1994).
- [22] S. Das, S. Samanta, R. Banik, R. Bhattacharjee, K. Basu, R. Raut, S. Ghugre, A. Sinha, S. Bhattacharya, S. Imran, G. Mukherjee, S. Bhattacharyya, A. Goswami, R. Palit, and H. Tan, *Nucl. Instrum. Methods Phys. Res., Sect. A* **893**, 138 (2018).
- [23] D. Radford, *Nucl. Instrum. Methods Phys. Res., Sect. A* **361**, 297 (1995).
- [24] R. Bhowmik, S. Muralithar, and R. P. Singh, *Proc. DAE Symp. Nucl. Phys. B* **44**, 422 (2001).
- [25] A. Krämer-Flecken, T. Morek, R. Lieder, W. Gast, G. Hebbinghaus, H. Jäger, and W. Urban, *Nucl. Instrum. Methods Phys. Res., Sect. A* **275**, 333 (1989).
- [26] K. Starosta, T. Morek, C. Droste, S. Rohoziński, J. Srebrny, A. Wierzchucka, M. Bergström, B. Herskind, E. Melby, T. Czosnyka, and P. Napiorkowski, *Nucl. Instrum. Methods Phys. Res., Sect. A* **423**, 16 (1999).
- [27] L. Genilloud, H. Börner, F. Corminboeuf, C. Doll, S. Drissi, M. Jentschel, J. Jolie, J. Kern, H. Lehmann, and N. Warr, *Nucl. Phys. A* **662**, 3 (2000).
- [28] A. Johnson, H. Ryde, and S. A. Hjorth, *Nucl. Phys. A* **179**, 753 (1972).
- [29] S. Raman, C. Malarkey, W. Milner, C. Nestor, and P. Stelson, *At. Data Nucl. Data Tables* **36**, 1 (1987).
- [30] I. Hamamoto and H. Sagawa, *Nucl. Phys. A* **327**, 99 (1979).
- [31] G. B. Hagemann, I. Hamamoto, and W. Satuła, *Phys. Rev. C* **47**, 2008 (1993).
- [32] D. Sohler, I. Kuti, J. Timár, P. Joshi, J. Molnár, E. S. Paul, K. Starosta, R. Wadsworth, A. Algora, P. Bednarczyk, D. Curien, Zs. Dombrádi, G. Duchene, D. B. Fossan, J. Gál, A. Gizon, J. Gizon, D. G. Jenkins, K. Juhász, G. Kalinka *et al.*, *Phys. Rev. C* **85**, 044303 (2012).
- [33] B. M. Nyakó, J. Gizon, A. Gizon, J. Timár, L. Zolnai, A. J. Boston, D. T. Joss, E. S. Paul, A. T. Semple, N. J. O'Brien, C. M. Parry, A. V. Afanasjev, and I. Ragnarsson, *Phys. Rev. C* **60**, 024307 (1999).
- [34] D. Sohler, J. Timár, G. Rainovski, P. Joshi, K. Starosta, D. B. Fossan, J. Molnár, R. Wadsworth, A. Algora, P. Bednarczyk, D. Curien, Zs. Dombrádi, G. Duchene, A. Gizon, J. Gizon, D. G. Jenkins, T. Koike, A. Krasznahorkay, E. S. Paul *et al.*, *Phys. Rev. C* **71**, 064302 (2005).
- [35] W. Nazarewicz and S. L. Tabor, *Phys. Rev. C* **45**, 2226 (1992).
- [36] W. R. Phillips, I. Ahmad, H. Emling, R. Holzmann, R. V. F. Janssens, T.-L. Khoo, and M. W. Drigert, *Phys. Rev. Lett.* **57**, 3257 (1986).
- [37] W. Urban, R. M. Lieder, W. Gast, G. Hebbinghaus, A. Krämer-Flecken, K. P. Blume, and H. Hübel, *Phys. Lett. B* **185**, 331 (1987).
- [38] S. J. Zhu, Q. H. Lu, J. H. Hamilton, A. V. Ramayya, L. K. Peker, M. G. Wang, W. C. Ma, B. R. S. Babu, T. N. Ginter, J. Kormicki, D. Shi, J. K. Deng, W. Nazarewicz, J. O. Rasmussen, M. A. Stoyer, S. Y. Chu, K. E. Gregorich, M. F. Mohar, S. Asztalos *et al.*, *Phys. Lett. B* **357**, 273 (1995).
- [39] E. Garrote, J. L. Egido, and L. M. Robledo, *Phys. Rev. Lett.* **80**, 4398 (1998).
- [40] B. Ackermann, H. Baltzer, C. Ensel, K. Freitag, V. Grafen, C. Günther, P. Herzog, J. Manns, M. Marten-Tölle, U. Müller, J. Prinz, I. Romanski, R. Tölle, J. deBoer, N. Gollwitzer, and H. J. Maier, *Nucl. Phys. A* **559**, 61 (1993).
- [41] N. V. Zamfir, P. von Brentano, and R. F. Casten, *Phys. Rev. C* **49**, R605 (1994).
- [42] R. V. Jolos, N. Minkov, and W. Scheid, *Phys. Rev. C* **72**, 064312 (2005).
- [43] M. Dahlinger, E. Kankleit, D. Habs, D. Schwalm, B. Schwartz, R. Simon, J. Burrows, and P. Butler, *Nucl. Phys. A* **484**, 337 (1988).
- [44] J. Hughes, R. Tölle, J. De Boer, P. Butler, C. Günther, V. Grafen, N. Gollwitzer, V. Holliday, G. Jones, C. Lauterbach, M. Marten-Tölle, S. Mullins, R. Poynter, R. Simon, N. Singh, R. Tanner, R. Wadsworth, D. Watson, and C. White, *Nucl. Phys. A* **512**, 275 (1990).